From Molecules to Heat-Integrated Processes: Computer-Aided Design of Solvents and Processes Using Quantum Chemistry

Lorenz Fleitmann[1,2], Christoph Gertig[2], Jan Scheffczyk[2], Johannes Schilling[1], Kai Leonhard[2], and André Bardow[1,2,3,*]

Supporting Information available online

Solvents are key to many chemical and energy conversion processes. Solvents should be selected as part of process design, optimizing a process-level objective to account for the interactions between molecular properties and process performance. In this paper, we integrate the computer-aided molecular design of solvents with the design of heat-integrated processes for minimum utility demand. The process flowsheet is represented by thermodynamically accurate shortcut process models, encompassing the most common unit operations: extraction, distillation, absorption, and multiphase reaction. For each candidate solvent, we optimize the process considering heat integration and design solvents based on their process performance. All thermodynamic properties are predicted using quantum chemistry. The method is applied to two case studies: extraction-distillation and integrated carbon capture and utilization. In both studies, designed solvents improve process performance compared to literature benchmarks, where simpler heuristics lead to suboptimal choices. Thus, the results highlight the importance of integrating molecular and process design to achieve maximum process performance.

1 Introduction

Maximum performance of chemical plants requires systematic process design during the conceptual design stage. For systematic process design, various optimization-based methods have been developed in process systems engineering [1]. A chemical process involves various units and auxiliaries to transform raw materials into products. Today, process design therefore includes the optimization of process settings and unit operations as well as heat recovery and utility systems [2] and the selection of molecules as auxiliaries such as solvents or working fluids [3–6].

Traditionally, process design follows a sequential approach from the reactor to separation and recycle systems and the heat exchanger network without explicitly considering auxiliaries [7]. However, this sequential approach does not account for the considerable interactions between the entire process system and each unit or the heat recovery subsystem. The optimal process system performance cannot always be achieved by separately optimizing the process subsystems. Thus, advanced design methods integrate the subsystems of the process flowsheet, e.g., by mathematical

optimization [8]. However, current methods focus either on (1) energy and mass integration or (2) solvent selection.

---

[1]Lorenz Fleitmann https://orcid.org/0000-0002-6350-5116, Dr. Johannes Schilling, https://orcid.org/0000-0001-8013-5439, Prof. Dr. André Bardow https://orcid.org/0000-0002-3831-0691, (abardow@ethz.ch)
ETH Zürich, Department of Mechanical and Process Engineering, Energy and Process Systems Engineering, Tannenstrasse 3, 8092 Zürich, Switzerland.
[2]Lorenz Fleitmann https://orcid.org/0000-0002-6350-5116, Christoph Gertig https://orcid.org/0000-0002-0959-1746, Dr. Jan Scheffczyk, Prof. Dr. rer. nat. Kai Leonhard
https://orcid.org/0000-0001-6231-6957,
Prof. Dr. André Bardow https://orcid.org/0000-0002-3831-0691 RWTH Aachen University, Institute of Technical Thermodynamics, Schinkelstraße 8, 52062 Aachen, Germany.
[3]Prof. Dr. André Bardow https://orcid.org/0000-0002-3831-0691 Forschungszentrum Jülich GmbH, Institute of Energy and Climate Research (IEK-10), Wilhelm-Johnen-Straße, 52425 Jülich, Germany.

1) Energy and mass integration: In the literature, several solutions are presented to integrate process optimization with the design of the heat recovery network [9–14]. These methods simultaneously design the (reaction-) separation process and heat exchange by solving large superstructure optimization problems. Superstructure problems usually contain nonconvexities and many discrete degrees of freedom and are thus challenging to solve [8]. Therefore, the solution methods often require tailored solution algorithms for computational efficiency. Recently, Liesche et al. [15] and Schack et al. [16] presented the superstructure-based process synthesis method FluxMax that avoids non-linearities in the optimization problem by discretizing the thermodynamic state space before optimization. Thereby, the non-linear process synthesis problem is reduced to a linear flux optimization of elementary process functions on the thermodynamic grid.

2) Solvent selection: Aside from process settings and heat integration, the performance of chemical and energy conversion processes is substantially impacted by the molecules used as auxiliaries, e.g., solvents [4, 17]. However, process design approaches considering heat integration usually assume a fixed selection of molecules or a small preselected set to avoid the problem complexity due to the large molecular design space [5].

However, process and solvent cannot be optimized independently and need to be integrated [3, 5, 6]. Choosing an optimal solvent is frequently key to the success of process design since only the optimal solvent enables maximum process performance. The selected solvent influences process conditions and optimal settings of unit operations and thus even heat integration and utility consumption.

Thus, various approaches have been developed for integrated computer-aided molecular and process design (CAMPD) to systematically evaluate the molecular design space for optimal combinations of molecules and processes [6, 18]. CAMPD methods link a molecular representation with a predictive thermodynamic model and a process model to account for the impact of molecular structure decisions on the process performance [3]. Because of the usually non-ideal thermodynamics and integer decision on the molecular structure, CAMPD problems are highly nonlinear and computationally challenging [18, 19]. Therefore, CAMPD methods commonly simplify either the process design scope or the molecular design space.

Many CAMPD methods approximate the solvent influence on the process using simplified performance indicators such as partition coefficients or relative volatilities [20–24]. Other CAMPD methods assess only single process units or flowsheet subsystems [22, 25–31]. However, limiting the process modeling to simplified performance indicators, single-unit operations or small subsystems of the process flowsheet does not capture all flowsheet-inherent trade-offs. Simplifying the process design scope can thus lead to suboptimal solvent selection for the final optimized overall process flowsheet [3, 6]. Even more, the influence of a heat recovery system has been neglected in CAMPD [5].

CAMPD methods modeling the whole process flowsheet typically simplify the molecular design scope by simplifying property prediction [32, 33] or limiting the molecular design space to specific molecular groups [34–42]. These CAMPD methods rely on one or more group contribution (GC) methods for predicting thermodynamic properties of candidate molecules. GC methods have been shown to accurately predict various thermodynamic and non-conventional properties [43, 44]. However, group parameters are usually parametrized from experimental data and are not available for all kinds of molecules, in particular for higher-order groups [45]. Moreover, several GC methods are usually employed to cover all thermodynamic properties required for process design, e.g., for ideal-gas heat capacities, activity coefficients or enthalpies of vaporization. However, combining several GC methods and parameter sets can lead to inconsistent predictions and contradictions [45]. Thus, CAMPD preferentially requires consistent property prediction that does not limit the molecular design space, e.g., based on quantum chemistry [3].

In this work, we aim to advance molecular and process design beyond the simplification of process models while building on reliable thermodynamic data from a large molecular design space. We present a CAMPD method that integrates molecular and process design by (1) modeling the entire process flowsheet, (2) including heat integration, and (3) using thermodynamic properties from quantum chemical calculations. Our method designs molecules and processes for maximum process performance of the entire heat-integrated process flowsheets. Because of the CAMPD problem complexity, we combine models for thermodynamic property prediction and process design that balance details, scope, and computational effort.

Our CAMPD method is based on the COSMO-CAMPD framework for integrated molecular and process design using a genetic algorithm, COSMO-RS and pinch-based process models [25, 46]. COSMO-RS allows for computing liquid phase properties and transitions between gas and liquid phase. Compared to the original COSMO-CAMPD [25], we further extend property prediction by automated quantum chemistry and thermochemistry calculations for the ideal gas state, enabling us to predict ideal-gas heat capacities of solvents for calculating sensible heats and heat integration. We use computationally efficient pinch-based process models from literature for fast and accurate process design of entire process flowsheets, including extraction, distillation, and absorption [47–49] and multiphase equilibrium reactions [50]. To efficiently target the heat-integrated energy demand, we extend the framework by the transshipment model for heat integration [51]. As a result, the method designs solvents based on minimum utility demand while remaining computationally tractable.

To explain and demonstrate the extended COSMO-CAMPD method, this article is structured as follows: In Sect. 2, the integrated CAMPD problem is formulated as an optimization problem and the solution algorithm is

explained. We describe which models have been integrated and which methods were used. In Sect. 3, the extended COSMO-CAMPD method is applied to two case studies: an extraction-distillation process (Sect. 3.1) and an integrated carbon capture and utilization process (Sect. 3.2). COSMO-CAMPD is compared with the state of the art and highlight the new capabilities of the method before conclusions are drawn in Sect. 4.

2 Method: COSMO-CAMPD for Heat-Integrated Processes

The presented COSMO-CAMPD method integrates molecular and process design using quantum chemistry-based property prediction and shortcut process models for unit operations and heat integration. The method can be formulated as an optimization problem for maximum process performance:

$$
\begin{aligned}
\min_{x,y} f(x, y, \xi,\ \psi,\ \theta) \quad & \text{Objective function} \\[4pt]
\text{s.t. } \xi = g(y, \psi) \quad & \text{Transshipment model for heat integration} \\[4pt]
\psi = h(y, \theta) \quad & \text{Process model} \\[4pt]
\theta = j(x, y) \quad & \text{Model for predicting thermodynamic properties} \\[4pt]
0 = k(x) \quad & \text{Representation of molecules} \\[2pt]
c_1(x) \leq 0 \quad & \text{Molecular constraints} \\[2pt]
c_2(\theta) \leq 0 \quad & \text{Thermodynamic constraints} \\[2pt]
c_3(y, \theta) \leq 0 \quad & \text{Process constraints} \\[2pt]
x \in X \quad & \text{Molecular structure} \\[2pt]
y \in Y \quad & \text{Process settings}
\end{aligned}
\tag{1}
$$

In this optimization problem, we optimize the molecular structure x and the process variables y for a process design objective function $f(x, y, \xi, \psi, \theta)$, e.g., the exergy demand or the operating cost of the process. The objective function f may depend on the molecular structure x, process variables y, targets for heat integration ξ, process quantities ψ, and thermodynamic properties θ. To calculate the objective, we integrate models for heat integration, process, thermodynamic properties, and molecular structure:

1) For targets for heat integration ξ: The heat integration model $g(y, \psi)$ calculates maximum feasible heat integration and corresponding minimum demands of utilities ξ based on the process variables y (e.g., optimised temperatures in unit operations) and process quantities ψ from the process model h (e.g., heat and mass flows).

2) For process quantities ψ: The process model $h(y, \theta)$ combines individual models of unit operations and depends on process variables y and thermodynamic properties θ, e.g., activity coefficients, heat capacities or enthalpies of vaporisation.

3) For thermodynamic properties θ: The predictive thermodynamic models $j(x, y)$ calculate thermodynamic properties for process model evaluation depending on

the molecular structure x and process settings y, e.g., activity coefficients, vapour pressures or ideal gas heat capacities.

4) For representing the molecular structure x: The CAMD model $k(x)$ represents the molecules using 3D-fragments and ensures chemical feasibility, e.g., the octet rule.

The optimization of the integrated design problem is subject to constraints on the molecular level $c_1(x)$ (e.g., the maximum number of non-hydrogen atoms), thermodynamic constraints $c_2(\theta)$ (e.g., a minimum boiling point of the solvent), and process constraints $c_3(y, \theta)$ (e.g., limits on process variables). The constraints c_1, c_2 and c_3 increase computational efficiency of the algorithm by discarding candidate solvents as soon as possible before performing more extensive evaluations [38]. The individual models are combined for one method for molecular and process design (Fig. 1). For details on the implementation, as well as for further use, the full source code of the extended COSMO-CAMPD method is freely available at https://gitlab.ethz.ch/epse/molecular-design-public/cosmo-campd.

Solution algorithm: We integrate property prediction using quantum chemistry and process optimization into a molecular design algorithm [52] resulting in an evolutionary optimization procedure of four steps per iteration (Fig. 1): (1) generation of candidate solvents, (2) prediction of thermodynamic properties, (3) process optimization and (4) ranking of candidate solvents.

1) Generation of candidate solvents: As the first step of each iteration, candidate solvents are generated using the genetic algorithm LEA3D [52]. The genetic algorithm forms the outer loop of the optimization procedure and runs property prediction (Step 2) and process optimization (Step 3) for each candidate solvent (Fig. 1). The genetic algorithm is based on a predefined 3D-molecular fragment library. LEA3D creates candidate solvents by combining molecular fragments. The initial generation is randomly created. Every subsequent generation is created by altering the candidate solvents of the previous generation through genetic operations, i.e., crossover and mutation. In this way, the genetic algorithm moves through the molecular design space.

   At any time, the candidate solvents from LEA3D satisfy chemical feasibility expressed through the equality constraints $k(x)$. The molecular constraints $c_1(x)$ are also checked by LEA3D for every candidate solvent. Candidate solvents violating the molecular constraints are discarded from further evaluation.

2) Prediction of thermodynamic properties: For each candidate solvent, thermodynamic properties θ are predicted based on quantum chemistry. To evaluate a process for operating cost or thermodynamic performance, equilibrium properties and thermochemical properties are required. For this purpose, we employ two quantum chemistry-based methods: COSMO-RS [53] for equilibrium properties (Sect. 2.1) and automated thermochem-

istry calculations for thermochemical properties (Paragraph 2.2).

2.1) COSMO-RS predicts equilibrium properties of pure components and mixtures, e.g. activity or Henry coefficients or enthalpies of vaporization. We use COSMO-RS on the TZVP-MF level of theory for each molecule, i.e., full geometry optimization and determination of the screening charge density (σ-surface) using the DFT functional BP86 and a TZVP basis set performed on a semiempirical conformer generation [53]. TZVP-MF exhibits a good balance between computational cost and accuracy for application in CAMPD [24]. The optimized geometries and σ-surface are computed for pure components and are stored in a local database for reuse. Thus, the time-consuming DFT calculations are only performed once for each candidate solvent.

Based on the thermodynamic equilibrium properties, property constraints $c_2(\theta)$ on thermodynamic requirements are evaluated, e.g., limits for boiling points or the existence of azeotropes [54]. Only "thermodynamically feasible" candidates are further considered for thermochemical calculations and process optimization.

2.2) Thermochemistry is used to calculate ideal gas properties, i.e., ideal gas heat capacities. Based on the preoptimized geometries from BP86/TZVP calculations, the molecular geometries are optimized, and vibrational frequencies are computed using the DFT functional B3LYP [55, 56] with TZVP basis set assuming the rigid rotor harmonic oscillator (RRHO) approximation [57]. B3LYP is more accurate than BP86 for geometry optimization as well as vibrational frequencies and is known for a good balance between computational cost and accuracy [58, 59]. Based on the optimized geometries and the vibrational frequencies, frequency analysis is performed using the TAMkin package [60] to yield the thermochemical properties.

Details on the software used for the quantum chemistry calculations and a brief comparison of the property prediction accuracy with experimental data can be found in the Supporting Information (SI) Sect. S1 and S3.

3) Process optimization: Using the thermodynamic properties from Step 2, we model the entire process flowsheet and optimize process settings using shortcut process models for individual process units (3.1) and heat integration (3.2).

3.1) Process units are modeled using equilibrium- and pinch-based process models. Pinch-based process models are available for the most common separation unit operations: absorption [48], extraction [49], and distillation [47]. An equilibrium-based multiphase reactor from Scheffczyk et al. [50] is

available using the homotopy continuation algorithm by Bausa and Marquardt [61] for phase equilibrium calculations. These equilibrium- and pinch-based shortcut process models allow modeling of entire process flowsheets for many processes.

The pinch-based shortcut process models are well suited for CAMPD since they consider non-ideal thermodynamics without simplifications to heuristic performance indicators (see Supporting Information Section S4 for a brief comparison to rigorous process models). Nevertheless, the calculation of process units is efficient and robust, e.g., by avoiding tray-to-tray calculations. Instead, pinch-based process models calculate the minimum operating point of a column by assuming vanishing thermodynamic driving forces. This assumption corresponds to columns with an infinite number of trays. Thus, in the context of balancing operating and investment expenditures, the results of the pinch-based models represent the limiting case of minimal operating expenditures without considering investment cost. CAMPD using pinch-based process models is suited to optimize thermodynamic quantities, e.g., exergy loss, energy and solvent demand, or operating cost, e.g. cost of utility consumption.

3.2) Heat integration is performed by pinch analysis using the transshipment model of Papoulias and Grossmann [51]. The transshipment model yields the maximum heat integration of a thermodynamically optimal heat recovery network. Like the pinch-based process models for the unit operations, investment costs for the heat recovery network are not calculated but targets for minimum utility consumption based on heat and mass flows. Using the transshipment model allows formulating the heat integration problem model as a linear program (LP) and solving it computationally efficiently. Thus, in combination with the pinch-based process models, maximum heat-integrated process performance is evaluated for each solvent based on a process-level objective function. The transshipment model and its mathematical optimization formulation are detailed for interested readers in Sect. S5 of the SI.

The used process models are computationally efficient and converge robustly compared to rigorous process models. Therefore, optimization of the process degrees of freedom, e.g., operating temperatures or pressures, is possible for each candidate solvent. Since the process models are black boxes for the overall CAMPD optimization algorithm, gradient-based numerical optimization from multiple starting points is employed (see SI Sect. S1 for details). For each evaluation of the objective function, the process flowsheet and heat integration is solved. The process optimization

yields optimal process settings considering subsequent heat integration for each solvent. Thus, each solvent can be evaluated in Step 4 based on its maximum process performance.

4) Ranking of molecules and next generation: Based on the results from process optimization, all candidate solvents are scored and ranked according to the predefined objective function. The objective function value is used as a fitness score for the genetic algorithm, which applies genetic operations to generate a new set of molecules (Step 1).

The four steps of the method are repeated until a predefined number of generations is met or a desired improvement is achieved, and the algorithm terminates. The result is a ranked list of molecules and corresponding optimal process settings that can be further refined by additional design criteria and validation. In this work, we check all candidate solvents of the ranked list for commercial availability or synthesizability. We verify commercial availability by searching online databases. If a candidate solvent is not commercially available, we check synthesizability using a retrosynthesis method based on the attention-based Molecular Transformer model [62, 63]. A candidate solvent is considered synthesizable if at most three subsequent reactions are required to form the candidate solvent from commercially available reactants with a confidence of the retrosynthesis algorithm greater than 50 %.

3 Case Studies and Application of COSMO-CAMPD

We apply the extended COSMO-CAMPD method to two case studies: (1) a hybrid extraction-distillation process for the purification of γ-valerolactone and (2) an integrated carbon capture and utilization (ICCU) process to produce carbon monoxide. The case studies demonstrate the capabilities of COSMO-CAMPD for integrated design of solvents and heat-integrated processes. In particular, we compare how the results from COSMO-CAMPD differ from state-of-the-art methods through extended property prediction using thermochemistry and heat integration.

3.1 Hybrid Extraction-Distillation of γ-Valerolactone

In recent years, the bio-based production of γ-valerolactone (GVL) from lignocellulosic biomass has been extensively discussed [64]. GVL is considered a promising platform chemical, a green solvent or even a renewable fuel. A production pathway for GVL via hybrid extraction-distillation of the aqueous reactor outlet (Fig. 2) has been proposed in the literature using the extraction solvent n-butyl acetate [65, 66]. Therefore, n-butyl acetate represents the benchmark for solvent design with COSMO-CAMPD in this work.

3.1.1 Problem Definition

The objective of the integrated solvent and process design is to minimize the process exergy demand after heat integration by choosing an optimal solvent with the corresponding optimal process settings. In this case study, the degrees of freedom of the process are the extraction and decanter temperatures T_{Extr} and T_{Dec} and the pressure in the distillation column p_{Dist}. The process modeling considers the reboiler and condenser duties in the distillation column, as well as the sensible heats for heating and cooling of various flows (Fig. 2). Heat is supplied by low-pressure (3 bar) and high-pressure (70 bar) steam at 410 K and 558.15 K, and cooling is provided by cooling water at 283 K. The heat recovery approach temperature (HRAT) is set to 10 K, and the feed is assumed to contain 5 mol % GVL. More details can also be found in the SI Sect. S6.

For the LEA3D algorithm, we limit the 3D molecular fragment library to fragments containing carbon, hydrogen, and oxygen to design potentially green and bio-based solvents (for details on the molecular fragments, see SI Sect. S2.1).
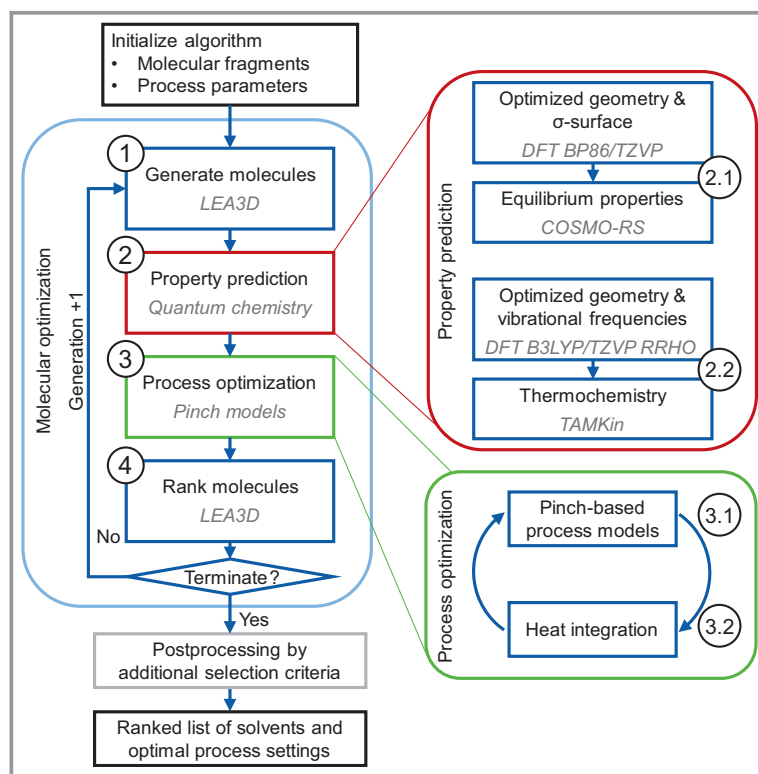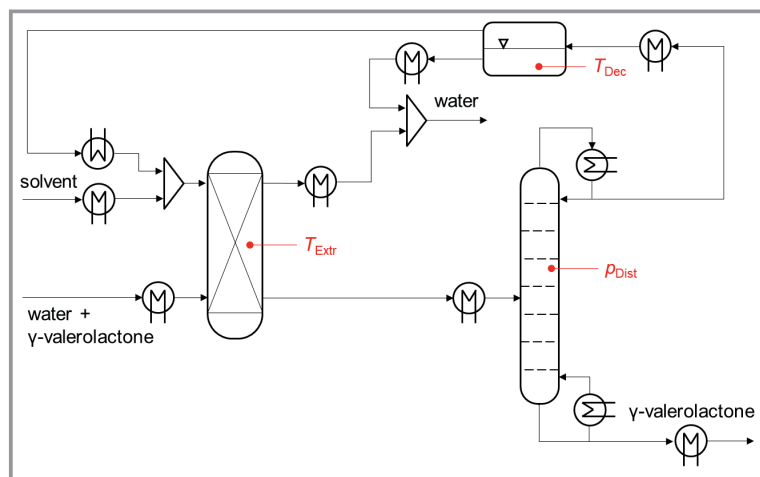

Figure 1. COSMO-CAMPD method for the design of heat-integrated processes by including thermochemistry from quantum chemistry calculations and process optimization including heat integration. The methods used are given in italics.

Figure 2. Flowsheet for the extraction-distillation of γ-valerolactone with process degrees of freedom highlighted for the process units.

3.1.2 Results and Discussion

In total, COSMO-CAMPD designs 715 unique candidate solvents in approximately 3.5 days. From the 715 candidate solvents, 348 candidate solvents fulfil the property constraints and are feasible as solvents for the process. 40 candidate solvents are neither commercially available nor predicted to be synthesizable as revealed by database search and retrosynthesis and thus are discarded after the design. The optimal solvent with the minimum exergy demand of the heat-integrated process is 3-vinylfuran. 3-vinylfuran leads to a total exergy demand of 43.7 kJ mol$_{GVL}^{-1}$ for the extraction-distillation process corresponding to a reduction in the exergy demand by 40 % compared to the benchmark *n*-butyl acetate with a total exergy demand of 72.9 kJ mol$_{GVL}^{-1}$. Besides 3-vinylfuran, the method designs 97 additional candidate solvents with a lower exergy demand than *n*-butyl acetate highlighting the systematic generation of promising alternatives. Of the top 50 candidate solvents, 42 candidate solvents contain the vinyl group or the furan group, which are thus identified as promising by the method. However, since molecules with vinyl groups tend to polymerize [67] and furanic compounds are suspected to be toxic and carcinogenic [68, 69], these candidates are subject to further, individual assessment. The most promising candidate solvent without a vinyl or furan group is toluene, with a total exergy demand of 55.0 kJ mol$_{GVL}^{-1}$, corresponding to a reduction by 25 % compared to *n*-butyl acetate.

Solvents for extraction-distillation processes are commonly selected using heuristic selection rules [3, 5, 6]. Thus, we compare the solvents identified using the heat-integrated exergy demand of the process as a selection criterion to solvents identified using standard selection rules from the literature. Commonly, heuristic selection rules for an extraction solvent focus only on the solvent's performance in the extraction column, e.g., the minimum solvent demand for extraction. From our analysis, the minimum solvent demand in extraction correlates well with the exergy demand of the heat-integrated process (Pearson's Correlation Coefficient $\rho = 0.92$, Fig. 3). Thus, we can confirm the heuristic that promising extraction solvents must necessarily exhibit a low solvent demand for extraction. However, this correlation does not apply among the high-ranking solvents, e.g., ranking higher than the benchmark n-butyl acetate. For these top 97 solvents, the correlation between the minimum solvent demand in extraction and the exergy demand of the heat-integrated process is weak (Pearson's Correlation Coefficient $\rho = 0.07$). Moreover, the solvent with the lowest solvent demand for extraction ranks only 182nd in total process exergy demand (Tab. 1). Therefore, the minimum solvent demand is not sufficient as objective to yield a low process exergy demand. The entire process needs to be considered for selecting an optimal extraction solvent.

Scheffczyk et al. [25] considered the combined extraction-distillation process and used the distillation reboiler energy demand as the objective of the solvent design. Since the authors did not include the thermochemical estimation of heat capacities for each candidate solvent, they did not consider sensible heats and heat integration. However, ranking the
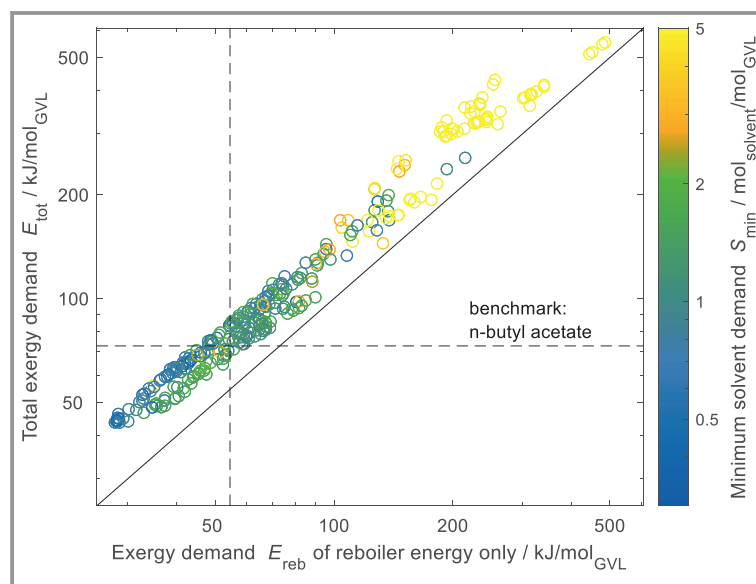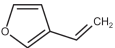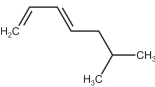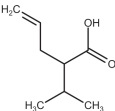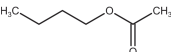

Figure 3. Comparison of total exergy demand of heat-integrated process (E_{tot}) and exergy demand from reboiler energy (E_{reb}) neglecting sensible heat. The color code indicates the heuristic selection criterion of minimum solvent demand for extraction (S_{min}).

Table 1. Highest ranking solvents for the extraction-distillation of γ-valerolactone based on the corresponding objective functions: Minimization of heat-integrated exergy demand of the entire process (E_{tot}), exergy demand of distillation reboiler neglecting sensible heat (E_{reb}) or solvent demand for extraction (S_{min}).

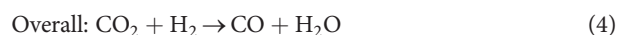| Optimal solvent regarding …	Molecular structure	Exergy demand process E_{tot}		Exergy demand reboiler E_{reb}		Solvent demand S_{min}	
		$\left[\text{kJ mol}_{GVL}^{-1}\right]$	Rank	$\left[\text{kJ mol}_{GVL}^{-1}\right]$	Rank	$\left[\text{mol mol}_{GVL}^{-1}\right]$	Rank
total heat-integrated exergy demand		43.7	1	28.6	11	0.036	42
exergy demand of distillation reboiler		43.7	2	27.8	1	0.032	30
solvent demand for extraction		97.7	182	80.2	200	0.021	1
benchmark n-butyl acetate		72.9	98	54.5	109	1.08	108

solvents designed for minimum heat-integrated exergy demand according to the objective function of Scheffczyk et al. [25] reveals only minor changes in solvent selection: The rankings are similar, as indicated by a rank correlation coefficient of ρ_{rank}= 0.98. Although heat integration reduces the total process exergy demand on average by 30 %, heat integration and more accurate modeling, including sensible heats, have a negligible effect on solvent design for the considered process flowsheet (Fig. 3). The reboiler duty, already calculated by Scheffczyk et al. [25], represents the main exergy demand of the process before and after heat integration since it cannot be heat integrated with this process. Therefore, designing solvents for minimum reboiler duty is sufficient for the process considered in this case study.

However, neglecting the sensible heat by using only the reboiler exergy demand underestimates the total heat-integrated process exergy demand on average by 29 %. In particular, the reboiler exergy demand is underestimated on average by 21 % because the additional heat demand from the temperature increase within the distillation column is not considered. Thus, accurate quantitative results require accurate process modeling including sensible heats and heat integration.

3.2 Integrated Carbon Capture and Utilization for the Production of Carbon Monoxide

Integrating carbon capture and utilization (ICCU) into one process can yield efficient process concepts to capture and utilize carbon dioxide (CO_2) as a feedstock for the chemical industry [70]. A promising CCU concept is the conversion of CO_2 with hydrogen (H_2) from fluctuating renewable energy to produce carbon monoxide (CO) via a storage molecule that compensates for the fluctuations in electricity

supply as a liquid energy carrier [71–73s]. In previous studies of Jens et al. [73] and Scheffczyk et al. [50], the most efficient process was achieved using dimethylformamide (DMF) as a storage molecule. DMF is produced in the synthesis reaction from CO_2, H_2 and dimethylamine (DMA, reaction 1) and subsequently reacted to form CO and dimethylamine in the reforming step (reaction 2):

$$\text{Reaction 1: } CO_2 + H_2 + DMA \rightarrow DMF + H_2O \tag{2}$$

$$\text{Reaction 2: } DMF \rightarrow CO + DMA \tag{3}$$

$$\text{Overall: } CO_2 + H_2 \rightarrow CO + H_2O \tag{4}$$

3.2.1 Problem Definition

So far, the described process has been investigated as a carbon capture and utilization process (CCU) with captured CO_2 as a pure feedstock for utilization. The potential of integrating the carbon capture from a CO_2 point source, e.g., CO_2-rich natural gas, by physical absorption has not yet been evaluated for this ICCU process. An ICCU process omits the energy-intensive CO_2 desorption step from the solvent by converting the CO_2 to a valuable product directly within the solvent. However, instead, the final product needs to be separated from the solvent.

As a result, the process performance of this ICCU process is substantially impacted by solvent and process design, as unit operations for physical absorption, reaction, and distillation are included in the process flowsheet and influenced by the employed solvent (Fig. 4). Therefore, the optimal solvent needs to balance various properties: (1) High absorption capacity and selectivity, (2) shift of the reaction equilib-

rium and phase split with water to allow catalyst recovery, as well as (3) low energy demand for heating, cooling, and separation in distillation. For each candidate solvent, the process design is tailored by optimizing the reactor pressure p_{Rx}, the pressures in the distillation columns p_{Dist1} and p_{Dist2} and the molar flow of water to the reactor $\dot{n}_{H_2O}$ to ensure phase separation. The optimization objective is minimizing the overall process exergy demand E_{tot} per mole CO normalized by the Gibbs free energy of the overall reaction $\Delta_R G^0_{CO}$:

$$\min E_{tot} = \frac{\sum_i \dot{Q}_i \left(1 - \frac{T_u}{T_i} \right)}{\dot{n}_{CO} \, \Delta_R G^0_{CO}} \tag{5}$$

with $\dot{Q}_i$ and T_i representing the heat duties and corresponding temperatures of the utilities, respectively. The overall reaction is the reverse water gas shift reaction, totalling in an overall Gibbs free energy of the reaction of $\Delta_R G^0_{CO} = 27.72 \text{ kJ mol}^{-1}$[73].

In contrast to the first case study (Sect. 3.1), in this design, we allow halogens, sulfur, and tertiary amines as building blocks for the LEA3D algorithm (see SI Sect. S2.2). These groups are expected to be inert. We limit the choice of amines to tertiary amines, which are not reactive in dry CO_2 capture [74, 75], as considered here. However, tertiary amines can catalyze the formation of bicarbonates from CO_2 in the presence of water [74, 75]. The effect of bicarbonate formation on CO_2 capture due to water impurities and water formation in the reaction is subject to refined evaluation and not considered in the present study. We also remove fragments with non-aromatic carbon double bonds, as these would be hydrogenated in the reactor. Thus, other reactions than reactions 1 and 2 are not assumed to occur.

Similar to the first case study (Sect. 3.1), heat that is not provided by heat integration is supplied by external utilities. Here, we assume low-pressure steam (3 bar) at 410 K and furnace heat at 750 K, as well as cooling water at 283 K and refrigeration at 233 K. The heat recovery approach temperature (HRAT) equals 10 K. As the CO_2 point source, we assume CO_2-rich natural gas with 30 mol % CO_2 and 70 mol % methane [70]. More details can also be found in the SI Sect. S6.

We compare the optimized ICCU process with an optimized separated CCU process from the literature, going forward called benchmark process. The CCU process uses the solvent dimethylpiperidine [73]. For separated carbon capture, we assume conventional chemical absorption using monoethanolamine [76].

3.2.2 Results and Discussion

The COSMO-CAMPD algorithm generates 1162 unique candidate solvents in approximately 9.5 days. Of these candidate solvents, 390 solvents are feasible for the ICCU process, and 330 candidate solvents are additionally commercially available or synthesizable as determined by database search or retrosynthesis. As the optimal solvent, the method discovers 5-fluoro-dimethylpentan-1-amine with an exergy demand of 148 kJ mol$^{-1}_{CO}$, which corresponds to 5.3 $\Delta_R G^0_{CO}$. Thus, the optimal solvent for the ICCU process reduces the exergy demand by 38 % compared to the benchmark separated CCU process with an exergy demand for this case study of 238 kJ mol$^{-1}_{CO}$, equalling 8.6 $\Delta_R G^0_{CO}$. This tertiary amine solvent would need to be further evaluated regarding the impact of water.

The best commercially available solvent is (difluoromethyl)benzene, ranking sixth with an exergy demand of 5.9 $\Delta_R G^0_{CO}$, which is 10 % higher than the exergy demand
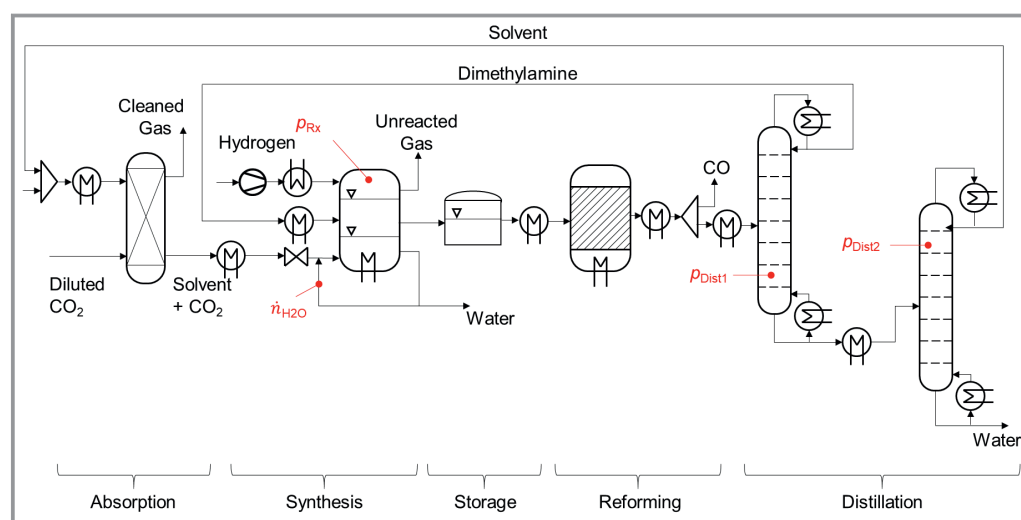

Figure 4. Flowsheet for the integrated carbon capture and utilization process producing carbon monoxide via the liquid energy carrier dimethylformamide. Dimethylformamide is produced in the synthesis reaction, stored, and reformed to carbon monoxide in the reforming step.

of the optimal solvent 5-fluoro-dimethylpentan-1-amine. In total, the method designs 176 candidate solvents with a lower exergy demand than the benchmark that are commercially available or synthesizable. Therefore, with an optimal combination of process and solvent, the ICCU process concept is an efficient alternative to the separated process and advantageous in terms of exergy demand. Nevertheless, about half of all evaluated solvents cause a higher exergy demand for the ICCU process than the benchmark separated process. Thus, as already highlighted by Jens et al. [70] for the feed specifications, an ICCU process cannot guarantee a lower exergy demand in general but requires careful and integrated solvent and process design as a key design decision.

We compare the solvent design based on the total heat-integrated process exergy demand to solvent rankings considering process subsystems only, i.e., unit operations. Generally, a higher absorption selectivity of the solvent for CO_2 leads to a higher yield in the reactor and thus to a lower total process exergy demand (cf. Fig. 5). This trade-off is confirmed by a correlation coefficient between the absorption selectivity and the total process exergy demand of $\rho = -0.54$. Similarly, a high equilibrium yield of dimethylformamide in the organic reactor outlet leads to a low exergy demand ($\rho = -0.66$). Importantly, equilibrium conversion does not correlate with exergy demand ($\rho = 0.01$) since primarily the product concentration in the organic phase at the reactor outlet impacts the separation effort but not generally equilibrium conversion alone.
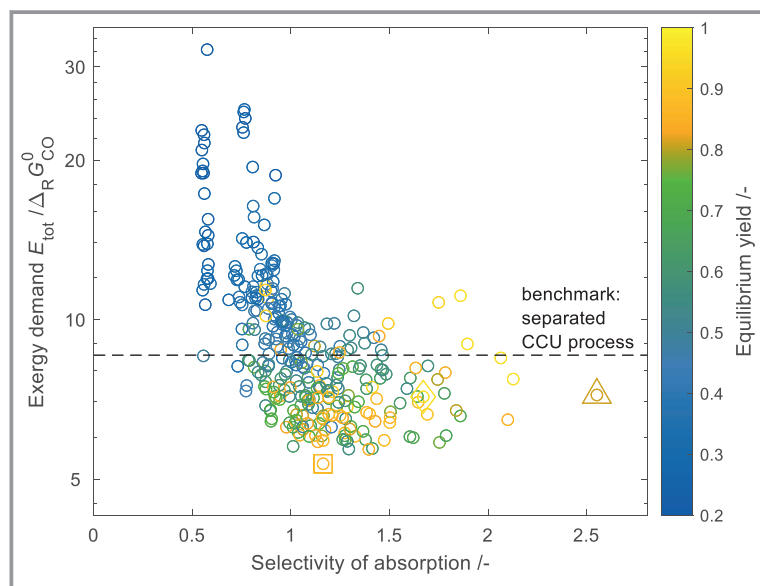
Despite the close correlation, choosing absorption selectivity or equilibrium yield as the design objective changes solvent selection: The solvent with the highest absorption selectivity is 2-phenylethanol (triangle in Fig. 5) and the solvent with the highest equilibrium yield is thiooxalane (diamond in Fig. 5). 2-phenylethanol and thiooxalane only rank 97th and 89th in total heat-integrated process exergy demand with exergy demands 34 % and 35 % higher than the optimal solvent 5-fluoro-dimethylpentan-1-amine (Tab. 2). Therefore, considering targets for single unit operations is not sufficient to select the optimal solvent for the overall process. Only an objective function based on the entire process successfully captures all process-relevant trade-offs within the molecular properties.

Heat integration strongly affects the total exergy demand of the process for every solvent. On average, heat integration reduces the total process exergy demand by 52 %, ranging from a minimum of 30 % to a maximum of 69 % of the total process exergy demand before heat integration (Fig. 6). Therefore, a quantitative estimation of the total exergy demand of the process requires the consideration of heat integration within the integrated design of process and solvent.
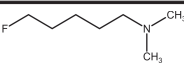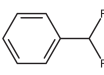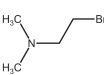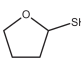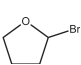
Heat integration also influences solvent ranking since the solvent properties impact the amounts of heat that can be integrated. However, considering the total process exergy demand without heat integration still enables differentiation between high- and low-ranking solvents. The correlation coefficient between solvent ranking with and without heat integration is $\rho_{rank} = 0.93$. Remarkably, for this case study, the separation exergy demand for distillation only is a good estimator for the total exergy demand of the heat-integrated process ($\rho = 0.90$). In separation, the candidate solvents exhibit substantial differences in the exergy demand. Thus, ranking according to separation effort is effective, although the separation exergy demand for distillation accounts for only 21 % of the total process exergy demand without heat integration on average.

In contrast to the low impact on the overall ranking, the heat integration potential significantly impacts solvent ranking among the top solvents. For example, when heat integration is not considered, only 33 candidates of the top 50 candidate solvents continue to be included in the revised top 50 candidate list. The correlation coefficient between solvent ranking with and without consideration of heat integration among the top 50 solvents is only $\rho_{rank} = 0.40$, indicating a weak correlation between the two rankings. Similarly, the correlation coefficient between total heat-integrated process exergy demand and exergy demand for distillation reduces to $\rho = 0.20$ for the top 50 candidate solvents.

When heat integration is considered in the design, the optimal solvent can successfully exploit increasing pressure in the distillation

Figure 5. Results of the integrated molecular and process design of the heat-integrated ICCU process: Each circle represents a molecular candidate with its corresponding optimized process. The candidate with the lowest heat-integrated process exergy demand is marked with a square, the candidate with the highest selectivity of absorption is marked with a triangle, and the candidate with the highest equilibrium yield is marked with a diamond.

Table 2. Ranking of candidate solvents based on the chosen objective function and exergy demand of the process normalized by the Gibbs free energy of the overall reaction $\Delta_R G_{CO}^0$ and the exergy demand of the solvent with the lowest total heat-integrated process exergy demand $E_{tot,1}$. The list contains the candidate solvent with the lowest total heat-integrated process exergy demand; the solvent with the lowest total heat-integrated process exergy demand commercially available; the solvent with the lowest total process exergy demand without heat integration; the solvent with the highest absorption selectivity and the solvent with the highest reactor equilibrium yield.

Solvent	Rank				Exergy demand	
	exergy demand		equilibrium yield	absorption selectivity	$E_{tot,i}/\Delta_R G_{CO}^0$	$E_{tot,i}/E_{tot,1}$
	with heat integration	without heat integration				
[structure]	1	17	27	106	5.34	1
[structure]	6	6	68	12	5.86	1.10
[structure]	10	1	22	31	5.92	1.11
[structure]	89	22	1	17	7.15	1.34
[structure]	97	69	56	1	7.21	1.35

columns to 2.7 and 4.1 bar for optimal heat integration. Thus, for this solvent, exergy demand decreases by 51 % from 11.0 $\Delta_R G_{CO}^0$ to 5.3 $\Delta_R G_{CO}^0$. In contrast, the optimal solvent without heat integration saves only 35 % of the process exergy demand by heat integration. As a result, the exergy demand after heat integration is 11 % higher than for the optimal solvent. Therefore, identifying the top solvents requires accurate modeling and consideration of heat integration.
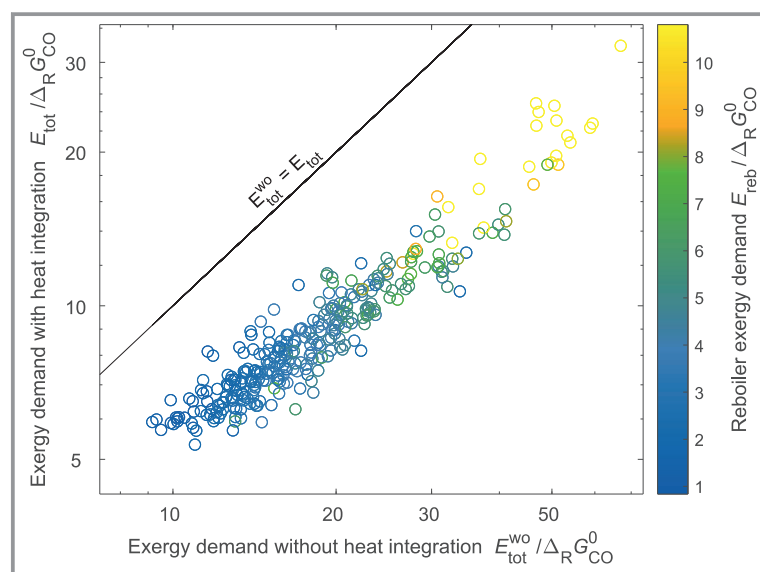
4 Conclusions

This paper presents the COSMO-CAMPD method for computer-aided, integrated molecular and process design for heat-integrated chemical processes. The method is based on a genetic algorithm that optimizes molecules evaluated by property prediction and process optimization. For all candidate solvents, we predict properties used in process optimization by quantum chemistry. Quantum chemistry allows the calculation of thermodynamic properties from a large molecular design space independent from the availability of parametrized functional groups. For computationally efficient and accurate process design, shortcut process models are used for extraction, absorption and distillation columns, and multiphase reaction. In addition, heat integration is considered for each candidate solvent within the process optimization. Therefore, process modeling and optimization overcome the limitations of state-of-the-art simplified process performance indicators often used in CAMPD.

Figure 6. Total process exergy demand considering process optimization with heat integration (E_{tot}) compared to a process optimization without considering heat integration potential (E_{tot}^{wo}) and the total reboiler exergy demand only (E_{reb}).

The method is applied to two case studies of (1) hybrid extraction-distillation and (2) integrated carbon capture and utilization. In both case studies, we design promising candidate solvents that are commercially available or synthesizable and reduce the process exergy demand by up to 40 % and 38 %, compared to literature benchmarks, respectively. Furthermore, the case studies reveal mutual dependencies of optimal solvents and processes. For optimal process performance, CAMPD requires a process-level objective that captures overall process performance, e.g., total heat-integrated process exergy demand. Separate consideration of individual unit operations or performance targets of process subsystems is not sufficient to design optimal solvents for the entire process, as evident by low correlation coefficients between the objective function values of the heuristics and the entire process.

The case studies show that heat integration significantly impacts quantitative estimates of, e.g., process exergy demand. Heat integration reduces the exergy demand in the case studies on average by 30 % and 52 %. Due to the large savings that can be achieved by heat integration depending on the candidate solvent, accurate modeling considering heat integration is crucial for selecting solvents for large process flowsheets with various unit operations. For the considered case studies, accurate ranking of promising candidate solvents cannot be achieved by simplified process representations. However, minimizing the main process energy drivers also provides a suitable selection criterion for generating promising candidates that should then be analyzed in subsequent detailed investigations.

The predictive methods still contain uncertainties that propagate through the presented CAMPD method. Therefore, valuable future work could quantify uncertainty in detail and explore potential improvements for CAMPD. Future work should also integrate further properties of solvents relevant for practical application that are currently not integrated or depend on manual inspection, e.g., inertness [77] or environment, health, and safety properties [78]. The presented method thus provides a strong basis for integrated molecular and process design and future extensions.

Supporting Information

Supporting Information for this article can be found under DOI: https://doi.org/10.1002/cite.202200098. This section includes additional references to primary literature relevant for this research [79–86].

CRediT authorship contribution statement

L.F.: Conceptualization, Methodology, Software, Validation, Investigation, Visualization, Writing – original draft, Writing – review & editing.
C.G.: Methodology, Software, Writing – review & editing.
Ja.S.: Conceptualization, Methodology, Validation, Visualization, Writing – review & editing.
Jo.S.: Conceptualization, Investigation, Visualization, Writing – review & editing.
K.L.: Methodology, Validation, Writing and review & editing, Supervision.
A.B.: Conceptualization, Methodology, Writing and review & editing, Supervision, Funding acquisition.

References

[1] E. N. Pistikopoulos, A. Barbosa-Povoa, J. H. Lee, R. Misener, A. Mitsos, G. V. Reklaitis, V. Venkatasubramanian, F. You, R. Gani, *Comput. Chem. Eng.* **2021**, *147*, 107252. DOI: https://doi.org/10.1016/j.compchemeng.2021.107252

[2] R. Smith, *Chemical process design and integration*, Wiley, Chichester **2005**.

[3] C. Gertig, K. Leonhard, A. Bardow, *Curr. Opin. Chem. Eng.* **2020**, *27*, 89–97. DOI: https://doi.org/10.1016/j.coche.2019.11.007

[4] T. Zhou, K. McBride, S. Linke, Z. Song, K. Sundmacher, *Curr. Opin. Chem. Eng.* **2020**, *27*, 35–44. DOI: https://doi.org/10.1016/j.coche.2019.10.007

[5] C. S. Adjiman, N. V. Sahinidis, D. G. Vlachos, B. Bakshi, C. T. Maravelias, C. Georgakis, *Ind. Eng. Chem. Res.* **2021**, *60 (14)*, 5194–5206. DOI: https://doi.org/10.1021/acs.iecr.0c05399

[6] S. Chai, Z. Song, T. Zhou, L. Zhang, Z. Qi, *Curr. Opin. Chem. Eng.* **2022**, *35*, 100732. DOI: https://doi.org/10.1016/j.coche.2021.100732

[7] J. M. Douglas, *AIChE J.* **1985**, *31 (3)*, 353–362. DOI: https://doi.org/10.1002/aic.690310302

[8] Q. Chen, I. E. Grossmann, *Annu. Rev. Chem. Biomol. Eng.* **2017**, *8*, 249–283. DOI: https://doi.org/10.1146/annurev-chembioeng-080615-033546

[9] J. Ryu, L. Kong, A. E. Pastore de Lima, C. T. Maravelias, *Comput. Chem. Eng.* **2020**, *133*, 106653. DOI: https://doi.org/10.1016/j.compchemeng.2019.106653

[10] X. Dong, Z. Liao, J. Sun, Z. Huang, B. Jiang, J. Wang, Y. Yang, *Ind. Eng. Chem. Res.* **2020**, *59 (46)*, 20455–20471. DOI: https://doi.org/10.1021/acs.iecr.0c04598

[11] C. Elsido, E. Martelli, I. E. Grossmann, *Comput. Chem. Eng.* **2019**, *128*, 228–245. DOI: https://doi.org/10.1016/j.compchemeng.2019.05.041

[12] C. Elsido, A. Mian, E. Martelli, *Energy Procedia* **2017**, *129*, 26–33. DOI: https://doi.org/10.1016/j.egypro.2017.09.171

[13] K. F. Kruber, T. Grüters, M. Skiborowski, *Comput. Chem. Eng.* **2021**, *147*, 107257. DOI: https://doi.org/10.1016/j.compchemeng.2021.107257

[14] L. Kong, S. M. Sen, C. A. Henao, J. A. Dumesic, C. T. Maravelias, *Comput. Chem. Eng.* **2016**, *91*, 68–84. DOI: https://doi.org/10.1016/j.compchemeng.2016.02.013

[15] G. Liesche, D. Schack, K. Sundmacher, *AIChE J.* **2019**, *65 (7)*, e16554. DOI: https://doi.org/10.1002/aic.16554

[16] D. Schack, G. Liesche, K. Sundmacher, *Chem. Eng. Sci.* **2020**, *215*, 115382. DOI: https://doi.org/10.1016/j.ces.2019.115382

[17] N. G. Chemmangattuvalappil, *Curr. Opin. Chem. Eng.* **2020**, *27*, 51–59. DOI: https://doi.org/10.1016/j.coche.2019.11.005

[18] A. I. Papadopoulos, I. Tsivintzelis, P. Linke, P. Seferlis, in *Elsevier Reference Module in Chemistry, Molecular Sciences and Chemical Engineering* (Eds: J. Reedijk), Elsevier, Waltham, MA **2018**.

[19] A. P. Samudra, N. V. Sahinidis, *AIChE J.* **2013**, *59 (10)*, 3686–3701. DOI: https://doi.org/10.1002/aic.14112

[20] T. Zhou, Z. Song, X. Zhang, R. Gani, K. Sundmacher, *Ind. Eng. Chem. Res.* **2019**, *58 (15)*, 5777–5786. DOI: https://doi.org/10.1021/acs.iecr.8b04245

[21] A. I. Papadopoulos, F. A. Perdomo, F. Tzirakis, G. Shavalieva, I. Tsivintzelis, P. Kazepidis, E. Nessi, S. Papadokonstantakis, P. Seferlis, A. Galindo, G. Jackson, C. S. Adjiman, *Chem. Eng. J.* **2020**, *420, Part 2*, 127624. DOI: https://doi.org/10.1016/j.cej.2020.127624

[22] N. D. Austin, N. V. Sahinidis, D. W. Trahan, *Chem. Eng. Sci.* **2017**, *159*, 93–105. DOI: https://doi.org/10.1016/j.ces.2016.05.025

[23] J. Ooi, D. K. S. Ng, N. G. Chemmangattuvalappil, *Ind. Eng. Chem. Res.* **2019**, *58 (29)*, 13210–13226. DOI: https://doi.org/10.1021/acs.iecr.9b01894

[24] J. Scheffczyk, L. Fleitmann, A. Schwarz, M. Lampe, A. Bardow, K. Leonhard, *Chem. Eng. Sci.* **2017**, *159*, 84–92. DOI: https://doi.org/10.1016/j.ces.2016.05.038

[25] J. Scheffczyk, P. Schäfer, L. Fleitmann, J. Thien, C. Redepenning, K. Leonhard, W. Marquardt, A. Bardow, *Mol. Syst. Des. Eng.* **2018**, *3 (4)*, 645–657. DOI: https://doi.org/10.1039/c7me00125h

[26] C. Gertig, L. Fleitmann, J. Schilling, K. Leonhard, A. Bardow, *Chem. Ing. Tech.* **2020**, *92 (10)*, 1489–1500. DOI: https://doi.org/10.1002/cite.202000112

[27] S. Jonuzaj, A. Gupta, C. S. Adjiman, *Comput. Chem. Eng.* **2018**, *116*, 401–421. DOI: https://doi.org/10.1016/j.compchemeng.2018.01.016

[28] S. Jonuzaj, C. S. Adjiman, *Chem. Eng. Sci.* **2017**, *159*, 106–130. DOI: https://doi.org/10.1016/j.ces.2016.08.008

[29] O. L. Watson, S. Jonuzaj, J. McGinty, J. Sefcik, A. Galindo, G. Jackson, C. S. Adjiman, *Org. Process Res. Dev.* **2021**, *25 (5)*, 1123–1142. DOI: https://doi.org/10.1021/acs.oprd.0c00516

[30] L. Zhang, J. Pang, Y. Zhuang, L. Liu, J. Du, Z. Yuan, *Chem. Eng. Sci.* **2020**, *226*, 115894. DOI: https://doi.org/10.1016/j.ces.2020.115894

[31] L. Fleitmann, J. Kleinekorte, K. Leonhard, A. Bardow, *Chem. Eng. Sci.* **2021**, *245*, 116863. DOI: https://doi.org/10.1016/j.ces.2021.116863

[32] X. Zhang, X. Ding, Z. Song, T. Zhou, K. Sundmacher, *AIChE J.* **2021**, *67 (10)*. DOI: https://doi.org/10.1002/aic.17340

[33] T. Zhou, Y. Zhou, K. Sundmacher, *Chem. Eng. Sci.* **2017**, *159*, 207–216. DOI: https://doi.org/10.1016/j.ces.2016.03.011

[34] J. Schilling, D. Tillmanns, M. Lampe, M. Hopp, J. Gross, A. Bardow, *Mol. Syst. Des. Eng.* **2017**, *2 (3)*, 301–320. DOI: https://doi.org/10.1039/c7me00026j

[35] J. Schilling, C. Horend, A. Bardow, *AIChE J.* **2020**, *66 (5)*, e16903. DOI: https://doi.org/10.1002/aic.16903

[36] F. E. Pereira, E. Keskes, A. Galindo, G. Jackson, C. S. Adjiman, *Comput. Chem. Eng.* **2011**, *35 (3)*, 474–491. DOI: https://doi.org/10.1016/j.compchemeng.2010.06.016

[37] J. Burger, V. Papaioannou, S. Gopinath, G. Jackson, A. Galindo, C. S. Adjiman, *AIChE J.* **2015**, *61 (10)*, 3249–3269. DOI: https://doi.org/10.1002/aic.14838

[38] S. Gopinath, G. Jackson, A. Galindo, C. S. Adjiman, *AIChE J.* **2016**, *62 (9)*, 3484–3504. DOI: https://doi.org/10.1002/aic.15411

[39] T. Keßler, C. Kunde, S. Linke, K. Sundmacher, A. Kienle, *Chem. Eng. Sci.* **2021**, *249*, 117243. DOI: https://doi.org/10.1016/j.ces.2021.117243

[40] L. M. van Kleef, O. A. Oyewunmi, C. N. Markides, *Appl. Energy* **2019**, *251*, 112513. DOI: https://doi.org/10.1016/j.apenergy.2019.01.071

[41] M. T. White, O. A. Oyewunmi, M. A. Chatzopoulou, A. M. Pantaleo, A. J. Haslam, C. N. Markides, *Energy* **2018**, *161*, 1181–1198. DOI: https://doi.org/10.1016/j.energy.2018.07.098

[42] M. T. White, O. A. Oyewunmi, A. J. Haslam, C. N. Markides, *Energy Convers. Manage.* **2017**, *150*, 851–869. DOI: https://doi.org/10.1016/j.enconman.2017.03.048

[43] A. S. Hukkerikar, B. Sarup, A. ten Kate, J. Abildskov, G. Sin, R. Gani, *Fluid Phase Equilib.* **2012**, *321*, 25–43. DOI: https://doi.org/10.1016/j.fluid.2012.02.010

[44] J. Marrero, R. Gani, *Fluid Phase Equilib.* **2001**, *183-184*, 183–208. DOI: https://doi.org/10.1016/S0378-3812(01)00431-9

[45] R. Gani, *Curr. Opin. Chem. Eng.* **2019**, *23*, 184–196. DOI: https://doi.org/10.1016/j.coche.2019.04.007

[46] L. Fleitmann, J. Scheffczyk, P. Schäfer, C. Jens, K. Leonhard, A. Bardow, *Chem. Eng. Trans.* **2018**, *69*, 559–564. DOI: https://doi.org/10.3303/CET1869094

[47] J. Bausa, R. v. Watzdorf, W. Marquardt, *AIChE J.* **1998**, *44 (10)*, 2181–2198. DOI: https://doi.org/10.1002/aic.690441008

[48] C. Redepenning, W. Marquardt, *AIChE J.* **2017**, *63 (4)*, 1213–1225. DOI: https://doi.org/10.1002/aic.15499

[49] C. Redepenning, S. Recker, W. Marquardt, *AIChE J.* **2017**, *63 (4)*, 1236–1245. DOI: https://doi.org/10.1002/aic.15523

[50] J. Scheffczyk, P. Schäfer, C. M. Jens, K. Leonhard, A. Bardow, *Comput.-Aided Chem. Eng.* **2017**, *40*, 1765–1770. DOI: https://doi.org/10.1016/B978-0-444-63965-3.50296-8

[51] S. A. Papoulias, I. E. Grossmann, *Comput. Chem. Eng.* **1983**, *7 (6)*, 707–721. DOI: https://doi.org/10.1016/0098-1354(83)85023-6

[52] D. Douguet, H. Munier-Lehmann, G. Labesse, S. Pochet, *J. Med. Chem.* **2005**, *48 (7)*, 2457–2468. DOI: https://doi.org/10.1021/jm0492296

[53] A. Klamt, F. Eckert, W. Arlt, *Annu. Rev. Chem. Biomol. Eng.* **2010**, *1*, 101–122. DOI: https://doi.org/10.1146/annurev-chembioeng-073009-100903

[54] M. Skiborowski, J. Bausa, W. Marquardt, *Ind. Eng. Chem. Res.* **2016**, *55 (24)*, 6815–6834. DOI: https://doi.org/10.1021/acs.iecr.6b01303

[55] P. J. Stephens, F. J. Devlin, C. F. Chabalowski, M. J. Frisch, *J. Phys. Chem.* **1994**, *98 (45)*, 11623–11627. DOI: https://doi.org/10.1021/j100096a001

[56] A. D. Becke, *J. Chem. Phys.* **1993**, *98 (7)*, 5648–5652. DOI: https://doi.org/10.1063/1.464913

[57] P. W. Atkins, R. Friedman, *Molecular quantum mechanics*, 5th ed., Oxford Univ. Press, Oxford **2011**.

[58] H. C. Gottschalk, A. Poblotzki, M. A. Suhm, M. M. Al-Mogren, J. Antony, A. A. Auer, L. Baptista, D. M. Benoit, G. Bistoni, F. Bohle, R. Dahmani, S. Firaha, S. Grimme, A. Hansen, M. E. Harding, M. Hochlaf, C. Holzer, G. Jansen, W. Klopper, W. A. Kopp, L. C. Kröger, K. Leonhard, H. Mouhib, F. Neese, M. N. Pereira, I. S. Ulusoy, A. Wuttke, R. A. Mata, *J. Chem. Phys.* **2018**, *148 (1)*, 14301. DOI: https://doi.org/10.1063/1.5009011

[59] J. Zheng, Y. Zhao, D. G. Truhlar, *J. Chem. Theory Comput.* **2009**, *5 (4)*, 808–821. DOI: https://doi.org/10.1021/ct800568m

[60] A. Ghysels, T. Verstraelen, K. Hemelsoet, M. Waroquier, V. van Speybroeck, *J. Chem. Inf. Model.* **2010**, *50 (9)*, 1736–1750. DOI: https://doi.org/10.1021/ci100099g

[61] J. Bausa, W. Marquardt, *Comput. Chem. Eng.* **2000**, *24 (11)*, 2447–2456. DOI: https://doi.org/10.1016/S0098-1354(00)00604-9

[62] P. Schwaller, T. Laino, T. Gaudin, P. Bolgar, C. A. Hunter, C. Bekas, A. A. Lee, *ACS Cent. Sci.* **2019**, *5 (9)*, 1572–1583. DOI: https://doi.org/10.1021/acscentsci.9b00576

[63] P. Schwaller, R. Petraglia, V. Zullo, V. H. Nair, R. A. Haeuselmann, R. Pisoni, C. Bekas, A. Iuliano, T. Laino, *Chem. Sci.* **2020**, *11 (12)*, 3316–3325. DOI: https://doi.org/10.1039/c9sc05704h

[64] Z. Zhang, *ChemSusChem* **2016**, *9 (2)*, 156–171. DOI: https://doi.org/10.1002/cssc.201501089

[65] S. Murat Sen, C. A. Henao, D. J. Braden, J. A. Dumesic, C. T. Maravelias, *Chem. Eng. Sci.* **2012**, *67 (1)*, 57–67. DOI: https://doi.org/10.1016/j.ces.2011.07.022

[66] J. Q. Bond, A. A. Upadhye, H. Olcay, G. A. Tompsett, J. Jae, R. Xing, D. M. Alonso, D. Wang, T. Zhang, R. Kumar, A. Foster, S. M. Sen, C. T. Maravelias, R. Malina, S. R. H. Barrett, R. Lobo, C. E. Wyman, J. A. Dumesic, G. W. Huber, *Energy Environ. Sci.* **2014**, *7 (4)*, 1500–1523. DOI: https://doi.org/10.1039/C3EE43846E

[67] H. Tobita, in *Ullmann's Encyclopedia of Industrial Chemistry*, Wiley-VCH Verlag, Weinheim **2000**.

[68] S. Moro, J. K. Chipman, J.-W. Wegener, C. Hamberger, W. Dekant, A. Mally, *Mol. Nutr. Food Res.* **2012**, *56 (8)*, 1197–1211. DOI: https://doi.org/10.1002/mnfr.201200093

[69] N. Bakhiya, K. E. Appel, *Arch. Toxicol.* **2010**, *84 (7)*, 563–578. DOI: https://doi.org/10.1007/s00204-010-0531-y

[70] C. M. Jens, L. Müller, K. Leonhard, A. Bardow, *ACS Sustainable Chem. Eng.* **2019**, *7 (14)*, 12270–12280. DOI: https://doi.org/10.1021/acssuschemeng.9b01603

[71] A. Behr, P. Ebbinghaus, F. Naendrup, *Chem. Eng. Technol.* **2004**, *27 (5)*, 495–501. DOI: https://doi.org/10.1002/ceat.200403221

[72] W. Supronowicz, I. A. Ignatyev, G. Lolli, A. Wolf, L. Zhao, L. Mleczko, *Green Chem.* **2015**, *17 (5)*, 2904–2911. DOI: https://doi.org/10.1039/c5gc00249d

[73] C. M. Jens, K. Nowakowski, J. Scheffczyk, K. Leonhard, A. Bardow, *Green Chem.* **2016**, *18 (20)*, 5621–5629. DOI: https://doi.org/10.1039/c6gc01202g

[74] R. Behrens, E. von Harbou, W. R. Thiel, W. Böttinger, T. Ingram, G. Sieder, H. Hasse, *Ind. Eng. Chem. Res.* **2017**, *56 (31)*, 9006–9015. DOI: https://doi.org/10.1021/acs.iecr.7b01937

[75] P. D. Vaidya, E. Y. Kenig, *Chem. Eng. Technol.* **2007**, *30 (11)*, 1467–1474. DOI: https://doi.org/10.1002/ceat.200700268

[76] U. Lee, J. Burre, A. Caspari, J. Kleinekorte, A. M. Schweidtmann, A. Mitsos, *Ind. Eng. Chem. Res.* **2016**, *55 (46)*, 12014–12026. DOI: https://doi.org/10.1021/acs.iecr.6b01668

[77] Q. Liu, L. Zhang, K. Tang, Y. Feng, J. Zhang, Y. Zhuang, L. Liu, J. Du, *Chem. Eng. Res. Des.* **2019**, *152*, 123–133. DOI: https://doi.org/10.1016/j.cherd.2019.09.018

[78] A. S. Alshehri, A. K. Tula, F. You, R. Gani, *AIChE J.* **2021**, e17469. DOI: https://doi.org/10.1002/aic.17469

[79] *COSMOconf16 (4.1)*, COSMOlogic GmbH & Co. KG, Leverkusen **2017**.

[80] *TURBOMOLE 7.2*, COSMOlogic GmbH & Co. KG, Leverkusen **2017**.

[81] *COSMOtherm17 (C30-1701)*, COSMOlogic GmbH & Co. KG, Leverkusen **2017**.

[82] M. J. Frisch, G. W. Trucks, H. B. Schlegel, G. E. Scuseria, M. A. Robb, J. R. Cheeseman, G. Scalmani, V. Barone, B. Mennucci, G. A. Petersson, H. Nakatsuji, M. Caricato, X. Li, H. P. Hratchian, A. F. Izmaylov, J. Bloino, G. Zheng, J. L. Sonnenberg, M. Hada, M. Ehara, K. Toyota, R. Fukuda, J. Hasegawa, M. Ishida, T. Nakajima, Y. Honda, O. Kitao, H. Nakai, T. Vreven, J. A. Montgomery Jr., J. E. Peralta, F. Ogliaro, M. Bearpark, J. J. Heyd, E. Brothers, K. N. Kudin, V. N. Staroverov, R. Kobayashi, J. Normand, K. Raghavachari, A. Rendell, J. C. Burant, S. S. Iyengar, J. Tomasi, M. Cossi, N. Rega, J. M. Millam, M. Klene, J. E. Knox, J. B. Cross, V. Bakken, C. Adamo, J. Jaramillo, R. Gomperts, R. E. Stratmann, O. Yazyev, A. J. Austin, R. Cammi, C. Pomelli, J. W. Ochterski, R. L. Martin, K. Morokuma, V. G. Zakrzewski, G. A. Voth, P. Salvador, J. J. Dannenberg, S. Dapprich, A. D. Daniels, O. Farkas, J. B. Foresman, J. V. Ortiz, J. Cioslowski, D. J. Fox, *Gaussian09 Rev. D.01*, Wallingford, CT **2009**.

[83] *MATLAB R2018b*, The MathWorks Inc., Natick, MA **2018**.

[84] J. S. Chickos, W. E. Acree, *J. Phys. Chem. Ref. Data* **2003**, *32 (2)*, 519–878. DOI: https://doi.org/10.1063/1.1529214

[85] S.-T. Lin, J. Chang, S. Wang, W. A. Goddard, S. I. Sandler, *J. Phys. Chem. A* **2004**, *108 (36)*, 7429–7439. DOI: https://doi.org/10.1021/jp048813n

[86] *NIST Chemistry WebBook: NIST Standard Reference Database Number 69* (Eds: P.J. Linstrom, W. G. Mallard), National Institute of Standards and Technology, Gaithersburg MD.